

Supporting Information

Real-time direct transmission electron microscopy imaging of phase and morphology transformation from solid indium oxide hydroxide to hollow corundum-type indium oxide nanocrystallites

Lukas Schlicker^{a*}, Radian Popescu^b, Maged F. Bekheet^a, Andrew Doran^c, Dagmar Gerthsen^b and Aleksander Gurlo^a

^[a] Fachgebiet Keramische Werkstoffe, Institut für Werkstoffwissenschaften und -technologien, Technische Universität Berlin, Hardenbergstr. 40, D-10623 Berlin

^[b] Laboratorium für Elektronenmikroskopie, Karlsruher Institut für Technologie (KIT), Engesserstr. 7, D-76131 Karlsruhe

^[c] Advanced Light Source, Lawrence Berkeley National Laboratory Berkeley, California 94720, USA

*Corresponding author

Synthesis

InOOH was synthesized solvothermally as reported elsewhere¹, upon calcination in air at 375-450°C InOOH decomposes to metastable rh-In₂O₃. Iron-doping is achieved by adding iron nitrate (Fe(NO₃) · xH₂O, Sigma-Aldrich) to the starting solution in atomic ratio In:Fe = 95:5 while keeping all other synthesis parameters unchanged.

In-situ XRD

The XRPD patterns shown in Fig 1e and patterns of the in-situ HT-XRPD study (Fig SI_Z) were recorded at the Advanced Light Source (Lawrence National Berkeley Labs, California, USA) in a Bragg-Brentano geometry using monochromatic synchrotron radiation with $\lambda=0.498538$ Å (25 keV / 30 μ m spot size). Sample powders were placed in 500 μ m fused silica capillaries and heated with 10 °/min in an infrared heated SiC tube furnace² to temperatures up to 1000°C while three XRPD patterns per minute were recorded. A Perkin Elmer flat panel detector (XRD 1621) with 26.315 °(2 θ) angular aperture was used to record the XRPD patterns with a step size of 0.018 °(2 θ). Wavelength and sample to detector distance was calibrated with the line positions of a LaB₆ standard in the program fit2d that was as well used for radial pattern integration^{3,4}.

Whole diffraction pattern fitting

Whole-diffraction-pattern fitting was applied to analyse the XRD data: the position and the integral breadth β - defined as the total area under the diffraction peak (hkl) divided by the peak intensity - of each diffraction line are determined after subtracting the linear interpolated background by fitting a Voigt function to its individual profile. The instrumental broadening was determined using the standard polycrystalline LaB₆ sample. The correction for the instrumental broadening is performed assuming Voigt profiles for the experimental h, the instrumental t and the physical f line profiles. The physical integral breadth β_f is calculated from the corresponding integral breadths β_h and β_t of the experimental and instrumental profile, respectively, by using an adequate formula for intermediate Gauss–Cauchy profiles:

$$\beta_f = \sqrt{(\beta_h - \beta_t) \sqrt{(\beta_h^2 - \beta_t^2)}}$$

The lattice parameter(s) of the nanomaterial is derived from the XRD line positions, while the volume-averaged particle size D_v and the average microstrains $\langle \varepsilon^2 \rangle^{1/2}$ are determined by the integral-breadth method using the physical integral breadth values β_f of all diffraction lines in the XRD pattern of the sample. Here, the separation of the particle size and microstrain contributions is carried out graphically within the average-size and strain approximation, by plotting $(\beta/k)^2$ as a function of β^2/k^2 [ref 5]. D_v is then obtained from the slope $m = 1/D_v$ of this graph, while the average microstrain is proportional to its intercept $n = (5\langle \varepsilon^2 \rangle^{1/2}/2)^2$. We point out that, for a sample composed of mono-crystalline spherical nanoparticles characterized by the volume-averaged diameter D_v , the real particle diameter D , which

is measured by TEM for example, is given by
$$D = \frac{4 \cdot D_v}{3}.$$

TEM / HRTEM

All TEM samples were prepared by dispersion of specimen powder in methanol and dropping this dispersion on a commercial 400 μm mesh Cu-grid (Plano 01824) covered by a holey amorphous carbon film, with a nominal thickness of 3 nm. The structure and the morphology of the synthesized specimens were investigated by high-resolution (HR) transmission electron microscopy (TEM), carried out on an aberration-corrected FEI Titan³ 80-300 microscope at 300 keV electron energy. Additional information about the crystalline structure of the nanocrystals (lattice parameters and crystal symmetry) was extracted from HRTEM images by calculating their two-dimensional Fourier transform (FT). Structure analysis was performed by comparing the experimental FT and calculated diffraction patterns using the Jems (Java version of the electron microscopy simulation) software [website: www.jems-saas.ch]. All reflections are marked and indexed in the FTs by using coloured circles and Miller indices, while the zero-order beam (ZB) is indicated by a white circle. Similarly, the crystal structure of nanoparticle ensembles was investigated from FTs calculated from HRTEM images. Such FTs show Bragg reflections on Debye-Scherrer rings, which are analysed in analogy to selected-area electron diffraction (SAED) patterns.

The distribution of different phases in single particles is visualized by Fourier-filtered (FF) images. For this purpose, the two-dimensional Fourier transform of a HRTEM image is calculated. A Bragg reflection (hkl) of the crystal structure of interest is selected in the FT image by centering a circular aperture around the reflection with a diameter equal to half of the minimal distance to its neighboring diffraction spots. The intensity of the selected Bragg reflection is artificially enhanced. A soft-edge filter in the FT image is applied to assure a smooth transition from the region with increased intensity around the selected reflection and the surrounding low-intensity background. The soft-edge aperture reduces artefacts in the FF image which would occur for an aperture with an abrupt transmission transition. An inverse two-dimensional FT is calculated only with the selected reflection. The FF image then reveals size and location of regions with the crystalline structure of interest within the specimen. This property of FF images is used to selectively enhance the contrast of crystalline domains with either InOOH or rh-In₂O₃ structure.

The size distribution of nanoparticles was determined from TEM images recorded at different magnifications by using a 2048×2048 pixel charge coupled device (CCD) camera and an exposure time of 0.5 s (Figure SI_4). For the evaluation of the diameter of solid quasi-spherical and hollow particles, the projected area of NPs on the TEM images was measured. The measured areas were evaluated by calculating the particle diameter with a circular projection area of the same size. These diameters were used to determine NP-size distributions in Figure SI 4. The average particle diameter is then calculated by fitting the calculated distributions with the lognormal size distribution function given by⁶:

$$f(D) = \frac{2}{D[2\pi \ln(1+c)]^{1/2}} \exp\left\{-\frac{\ln^2[DD^{-1}(1+c)^{1/2}]}{[2 \ln(1+c)]}\right\}$$

where \bar{D} is the average particle diameter and $c = \sigma_D^2/\bar{D}^2$ with σ_D the distribution dispersion.

The sphere-to-hollow-sphere and rod-to-tube transformation is investigated by using series of HRTEM images successively recorded during continuous illumination of the same sample region every 1 min, starting just after a given position on the sample is reached ($t=0$) and ending after 10 to 30 min. Advantage is taken from the fact, that InOOH particles (i.e. the initial spheres and rods) are not stable under irradiation with the high-energy electrons in the transmission electron microscope and undergo a phase and morphological transformation towards hollow In_2O_3 structures after 2 to 14 min. The final morphologies after electron-beam induced transformation are identical to the ones obtained by ex-situ calcination.

HAADF-STEM combined with EDXS

The morphology and the chemical composition of single nanoparticles as well as the average chemical composition of particle agglomerations was investigated by high-angle annular dark-field (HAADF) scanning transmission electron microscopy (STEM) combined with energy-dispersive X-ray spectroscopy (EDXS). The experiments were carried out with an FEI Osiris ChemiSTEM microscope with 200 keV electron energy. The instrument is equipped with a Bruker Quantax system (XFlash detector) for EDXS. EDX spectra were quantified with the FEI software package "TEM imaging and analysis" (TIA) version 4.7 SP3, applying a refined Kramers' law, which includes corrections for detector absorption and background subtraction. Standard-less quantification, i.e. by means of theoretical sensitivity factors, without thickness correction was applied. Additionally, EDXS elemental maps of In (In- $L_{\alpha 1}$ line), O (O- K_{α} line) and Fe (Fe- $K_{\alpha 1}$ line) were recorded and used to investigate the elemental distributions within individual nanoparticles. The EDXS elemental maps were analyzed by using the ESPRIT software (version 1.9, Bruker, Germany).

EDX spectra obtained during scanning rectangular areas inside a single particle or a particle ensemble are used to determine their average chemical compositions. However, the O concentration measured on a nanoparticle is the sum of the real O concentration within the nanoparticle and the O concentration on the substrate under the nanoparticle, which results from contamination with substances containing O, like e.g. water, etc. Then, the O concentration on the substrate was determined and subtracted from the total O concentration measured on nanoparticle(s) before calculating its (their) real composition. For that reason, EDXS area scans of substrate regions close to the investigated nanoparticle(s), were separately recorded and quantified. We note that hydrogen cannot be detected by EDXS.

Effect of electron-beam illumination on atom displacement and sample heating

The solid-to-hollow nanoparticle transition was investigated using an electron dose rate of $1.04 \cdot 10^6 \text{ e nm}^{-2} \text{ s}^{-1}$ and a beam current $I=9.7 \text{ nA}$. A slightly smaller dose rate of $0.89 \cdot 10^6 \text{ e} \cdot \text{nm}^{-2} \cdot \text{s}^{-1}$ and about the same beam current $I=9.6 \text{ nA}$ was used for the nanorod-nanotube transition.

The temperature increase by electron illumination can only be roughly estimated. We have used Eq.(1) given in ref. ⁷ to calculate the local temperature T compared to the surrounding temperature T_0 . Accordingly, the heat per second deposited in a sample (in our case a nanoparticle with diameter d) is given by $I \cdot \langle E \rangle \cdot (d/\lambda)$ with the beam current I in A, the average energy loss per inelastic collision $\langle E \rangle$ in eV and the mean free path λ in m for inelastic scattering. Under steady state condition, the heat generated by the incident electron beam with a diameter b (nm), is balanced by the heat loss due to radial conduction over a distance R_0 (nm) through a material with thermal conductivity K [7]:

$$I \cdot \langle E \rangle \cdot \frac{d}{\lambda} = \frac{4 \cdot \pi \cdot d \cdot K \cdot (T - T_0)}{0.58 + 2 \cdot \ln(2 \cdot R_0/b)} \quad (1)$$

Here, the heat loss due to radiation was neglected as suggested in [7]. For InOOH nanoparticles and nanorods, $R_0=300 \text{ nm}$ is experimentally determined as the distance measured on HRTEM images from the center of the illuminated region up to the region, where no structure/morphology change of nanoparticles was observed after illumination. A thermal conductivity value of $K=0.84 \text{ Wm}^{-1}\text{K}^{-1}$ (K of nanocrystalline $\text{rh-In}_2\text{O}_3$ was used because a value for InOOH is not available) [8], a mean free path $\lambda=115 \cdot 10^{-9} \text{ m}$ [9] and an average energy loss for inelastic collisions $\langle E \rangle=13.5 \cdot Z_m=223 \text{ eV}$ [10] ($Z_m=16.5$ the average atomic number of InOOH) is assumed for both types of InOOH nanoparticles. Under steady state conditions, a temperature difference $\Delta T=T-T_0=10 \text{ }^\circ\text{C}$ is calculated from Eq. (1) between the illuminated InOOH nanorod and the surrounding region for an electron beam diameter of $b=50 \text{ nm}$. For the InOOH nanoparticles a temperature difference $\Delta T=12 \text{ }^\circ\text{C}$ is calculated for corresponding beam diameter of $b=30 \text{ nm}$.

Knock-on damage by elastic electron-nucleus collisions also occurs during illumination by high-energy electrons and is treated in the following way: according to Seitz and Koehler [11], the maximum amount of energy T_m , which can be transferred by elastic scattering between an incident electron and a target atom is given by:

$$T_m = \frac{2 M E (E + 2mc^2)}{(M + m)^2 c^2 + 2ME} \quad (2)$$

where m is the electron mass and c is the light speed. E is the electron energy and M the mass of the target atom. According to Eq.(2), the maximum transferred energies at $E=300 \text{ keV}$ are $T_m = 7.4 \text{ eV}$ for In atoms, $T_m = 53.3 \text{ eV}$ for O atoms and of $T_m = 50.1 \text{ eV}$ for the OH-groups in InOOH.

The cross-section for knock-on (displacement) damage σ_k by the electrons can be calculated according to [11]:

$$\sigma_k = \left(\frac{Ze^2}{2\varepsilon_0 mc^2} \right)^2 \frac{1 - \beta^2}{4\pi\beta^4} \left\{ \frac{T_m}{E_d} - 1 - \beta^2 \ln\left(\frac{T_m}{E_d}\right) + \pi \frac{Ze^2}{\hbar c} \beta \left[2 \left(\frac{T_m}{E_d}\right)^{\frac{1}{2}} - \ln\left(\frac{T_m}{E_d}\right) - 2 \right] \right\} \quad (3)$$

with the vacuum permittivity constant ϵ_0 , the threshold energy for displacement of the target atom E_d , e is the electron charge and $\beta = v/c$ containing the electron velocity v .

Bond dissociation energy values of $\Delta E(\text{In-O})=318$ kJ/mol [12] for the In-O bond and $\Delta E(\text{In-OH})=360$ kJ/mol [12] for the In-OH bond are used to calculate threshold displacement energies of $E_d=3.5$ eV for In atoms, $E_d=3.3$ eV for O atoms and $E_d=3.7$ eV for OH-groups, respectively, in InOOH at room temperature. An average bond dissociation energy of $\Delta E=339$ kJ/mol is considered for the calculation of E_d of In by taking into account the presence of both, the In-O and In-OH bonding for In atoms in InOOH.

For a maximum transmitted energy of $T_m=7.4$ eV and $E_d=3.5$ eV, a displacement cross-section value of $\sigma_k=429.8$ barn ($1 \text{ barn}=10^{-24} \text{ cm}^2$) can be calculated for In atoms within InOOH by using Eq. (3). These data result in an expected average lifetime of 37 s of In atoms on their sites in InOOH nanorods before displacement due to illumination with high-energy electrons at an electron dose rate of $0.89 \cdot 10^6 \text{ e nm}^{-2} \text{ s}^{-1}$, and only 22 s for In atoms in InOOH nanoparticles under illumination with an electron dose rate of $1.04 \cdot 10^6 \text{ e} \cdot \text{nm}^{-2} \cdot \text{s}^{-1}$. Similarly, for $T_m=53.3$ eV and $E_d=3.3$ eV, a displacement cross-section of $\sigma_k=134.2$ barn is calculated from Eq. (3) for O atoms, while a $\sigma_k=188.8$ barn is determined for OH-groups by replacing in Eq. (3) its corresponding values for $T_m=50.1$ eV and $E_d=3.7$ eV. These result in lifetimes of 68 s and 41 s for O atoms on their sites in InOOH nanorods and nanoparticles, respectively, while lifetimes of 84 and 51 s are calculated for OH-groups before displacement.

Calculation of contraction factor

The (idealized) geometric volumes (see Fig. SI_0 for sketches) of the nanoparticles under investigation are given by: InOOH sphere volume with diameter D_{sphere} (Eq. 1) and the transformed In_2O_3 hollow sphere volume (Eq. 2) with outer diameter $D_{\text{h-sphere}}$ and inner diameter $d_{\text{h-sphere}}$:

$$V_{\text{InOOH-Sphere}} = \frac{1}{6} \pi D_{\text{sphere}}^3 \quad (\text{Eq. 1})$$

$$V_{\text{In}_2\text{O}_3\text{-hollow_sphere}} = \frac{1}{6} \pi (D_{\text{h-sphere}}^3 - d_{\text{h-sphere}}^3) \quad (\text{Eq. 2})$$

Iron doped InOOH rod volume with length L_{rod} and diameter D_{rod} (Eq. 3) and the In_2O_3 tube volume (Eq. 4) with length L_{tube} , outer diameter D_{tube} and inner diameter d_{tube} and sphere-like tube tips.

$$V_{\text{InOOH-rod}} = \frac{1}{4} \pi D_{\text{rod}}^2 (L_{\text{rod}} - D_{\text{rod}}) + \frac{1}{6} \pi D_{\text{rod}}^3 \quad (\text{Eq. 3})$$

$$V_{\text{In}_2\text{O}_3\text{-tube}} = \frac{1}{4} \pi (D_{\text{tube}}^2 - d_{\text{tube}}^2) (L_{\text{tube}} - D_{\text{tube}}) + \frac{1}{6} \pi (D_{\text{tube}}^3 - d_{\text{tube}}^3) \quad (\text{Eq. 4})$$

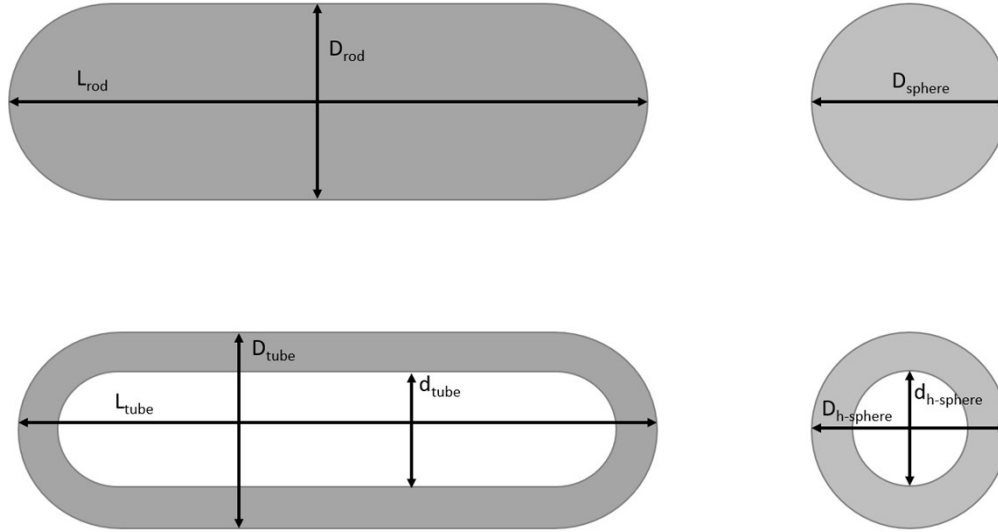


Figure SI_0: Sketch of rod, tube, sphere and hollow sphere with dimensions denoted.

The outside shape of spheres and rods as well as the rod length is maintained during transformation:

$$D_{sphere} = D_{h-sphere} \text{ (Eq. 5)}$$

$$D_{rod} = D_{tube} \text{ (Eq. 6)}$$

$$L_{rod} = L_{tube} \text{ (Eq. 7)}$$

With the average particle dimensions in [nm] as measured on several hundreds of nanoparticles (see particle size di-stributions and values listed in the article Table 1): $D_{h-sphere} = 18 \pm 4$; $d_{h-sphere} = 8 \pm 2$; $D_{tube} = 18 \pm 4$; $d_{tube} = 8 \pm 2$; $L_{min} = 30$ nm; $L_{max} = 570$ nm the observed and calculated contraction factors with errors in accordance to gaussian error propagation are:

$$\text{Sphere: } \sqrt[3]{\frac{V_{InOOH-sphere}}{V_{In2O3-hollow_sphere}}} = 1.031 \pm 0.033$$

$$\text{Rod: } \sqrt[3]{\frac{V_{InOOH-rod}}{V_{In2O3-tube}}} = 1.075 \pm 0.264 \text{ (} L = 570 \text{)} ; \sqrt[3]{\frac{V_{InOOH-rod}}{V_{In2O3-tube}}} = 1.052 \pm 0.381 \text{ (} L = 30 \text{)}$$

With $V_{InOOH-formula_unit} = 39.2 \text{ \AA}^3$ and $V_{In2O3-formula_unit} = 31.6 \text{ \AA}^3$ the ideal contraction factor is:

$$\text{Ideal: } \sqrt[3]{\frac{V_{InOOH-formula_unit}}{V_{In2O3-formula_unit}}} = 1.076$$

The measured contraction by the factors 1.031 ± 0.033 for the spherical particles and 1.075 ± 0.264 respectively 1.052 ± 0.381 for the rod like particles of maximum and minimum length are close to the theoretical value of 1.076 as calculated from the volumes occupied per formula unit in both structures.

Supporting Figures

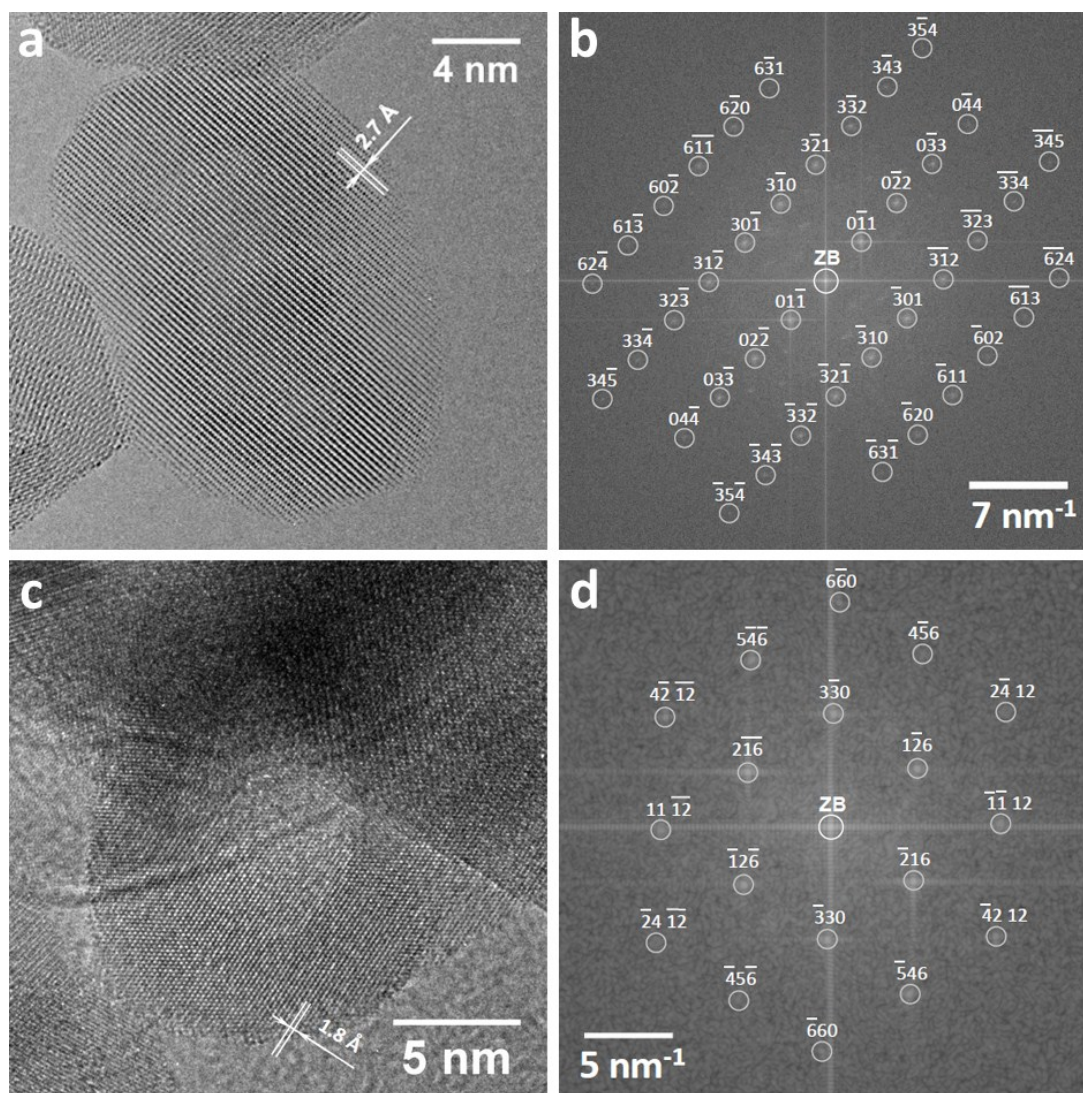


Figure SI_1: a) HRTEM image of a single InOOH nanoparticle; b) its Fourier transform (FT) and calculated diffraction pattern with Miller indices for the bulk orthorhombic InOOH (P21nm, No. 31, lattice parameters of $a=5.26 \text{ \AA}$, $b=4.56 \text{ \AA}$ and $c=3.27 \text{ \AA}$) in the [133]-zone axis; c) HRTEM image of a single rh-In₂O₃ hollow particle; d) its FT and calculated diffraction pattern with Miller indices for the bulk rhombohedral In₂O₃ (R-3cH, No. 167, lattice parameters of $a=5.49 \text{ \AA}$, $c=14.51 \text{ \AA}$) in the [661]-zone axis.

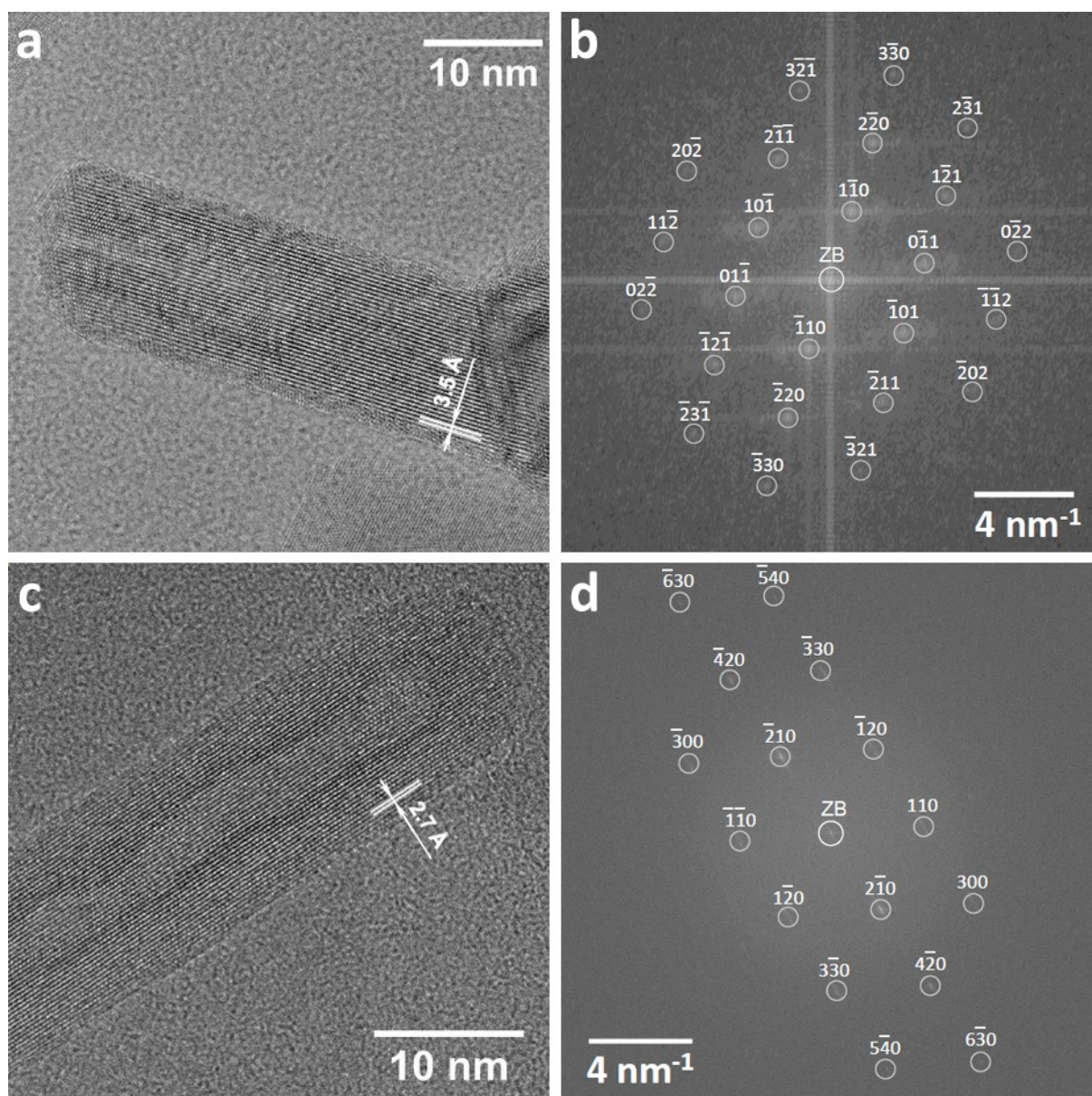


Figure SI_2: a) HRTEM image of a single $\text{In}_{0.97}\text{Fe}_{0.03}\text{OOH}$ nanorod; b) its Fourier transform (FT) and calculated diffraction pattern with Miller indices for the bulk orthorhombic InOOH (P21nm, No. 31) in the $[111]$ -zone axis; c) HRTEM image of a single $\text{In}_{1.94}\text{Fe}_{0.06}\text{O}_3$ tube; d) its FT and calculated diffraction pattern with Miller indices for the bulk rhombohedral In_2O_3 (R-3c, No. 167) in the $[001]$ -zone axis.

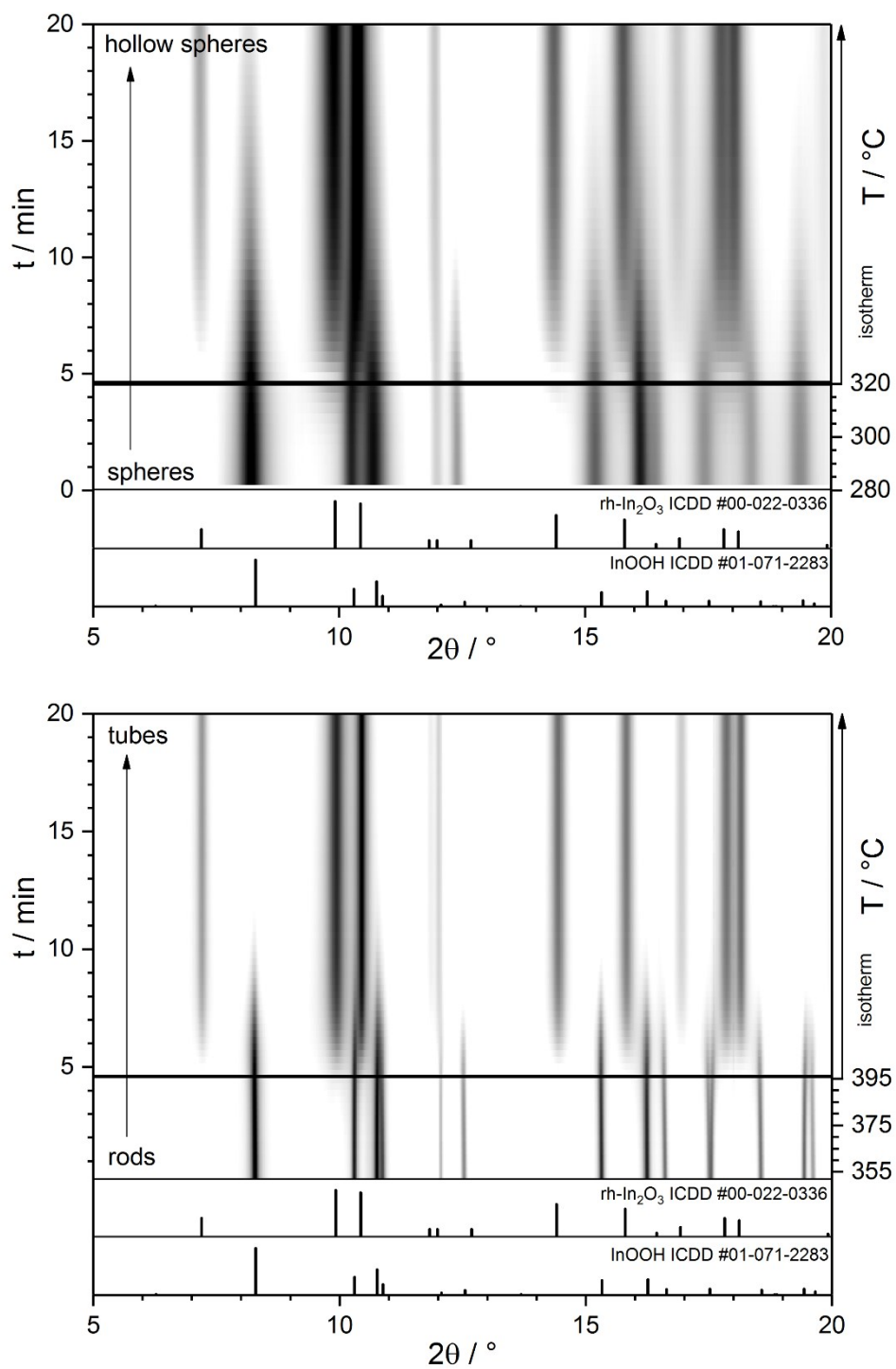


Figure SI_3: Time resolved in-situ heating synchrotron XRD study of the transformation of InOOH spheres (top) and rods (bottom) towards rh- In_2O_3 .

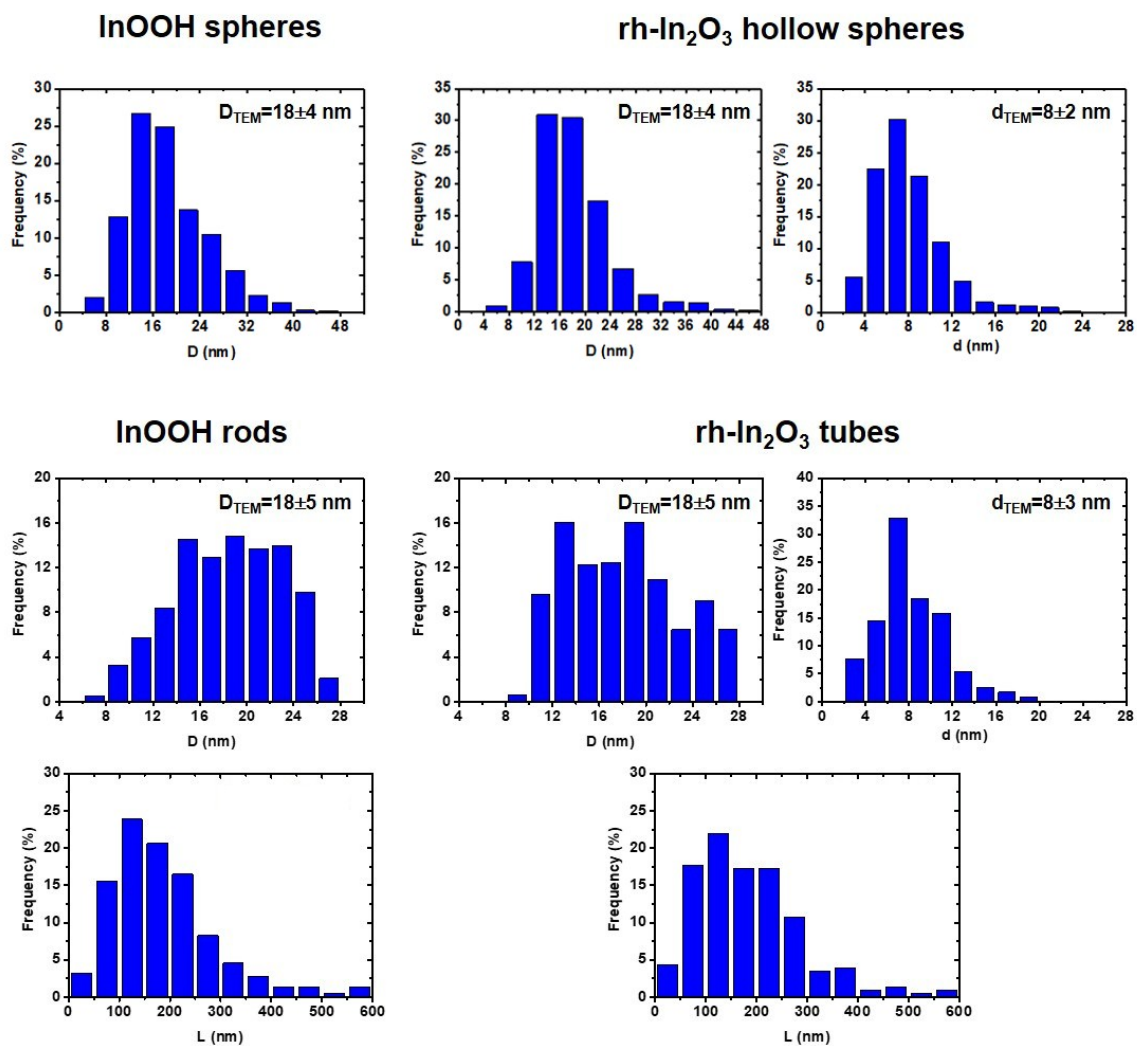


Figure SI_4: Experimental size distributions of nanoparticles derived from TEM measurements. The average outer (D) and inner (d) diameters of particles and rods/tubes are indicated within each distribution.

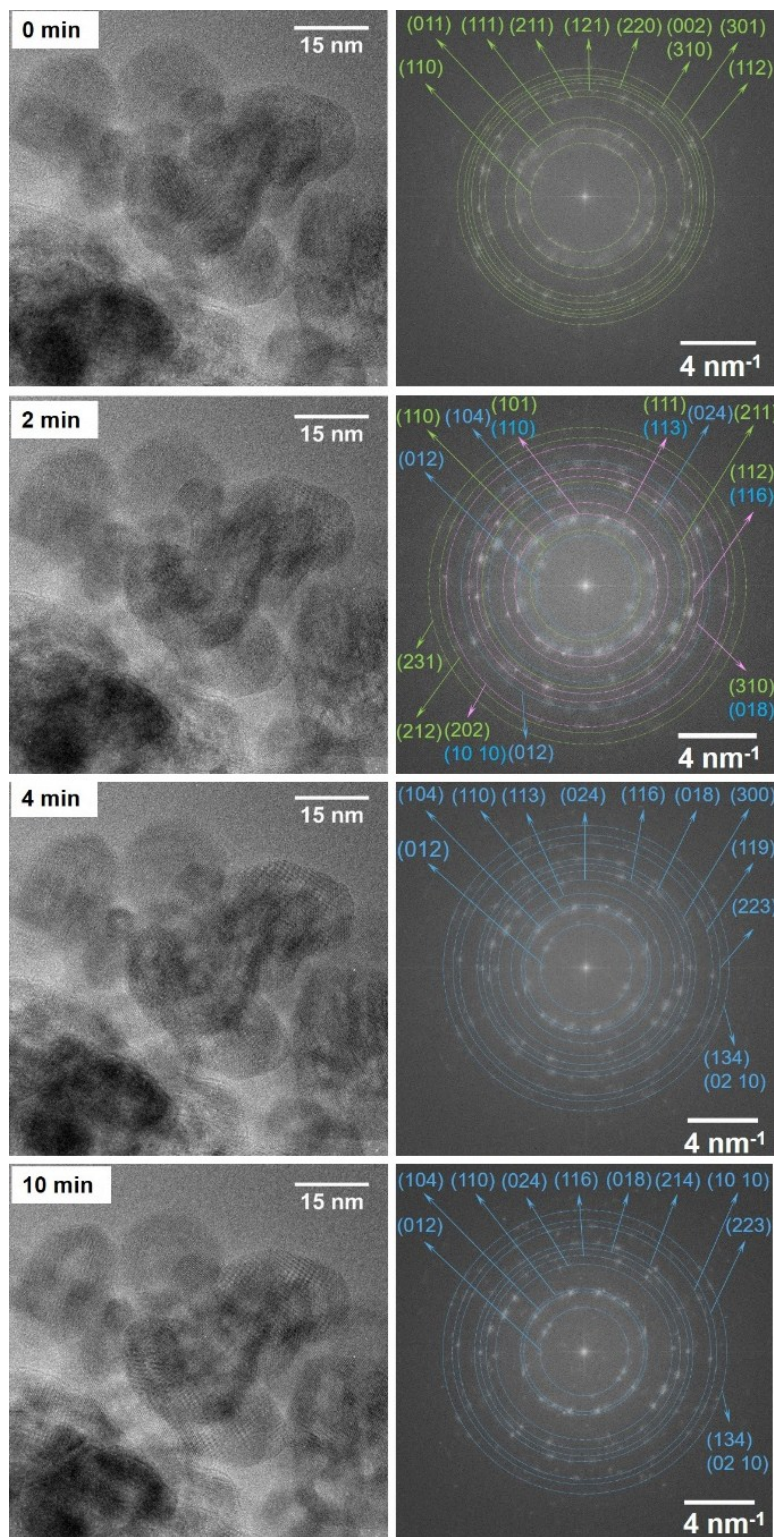


Figure SI_5: A series of HRTEM images and their corresponding indexed FT patterns recorded during the InOOH sphere to rh-In₂O₃ hollow sphere transformation for an ensemble of InOOH particles upon 300 keV electron beam irradiation in the transmission electron microscope (illumination time intervals are given in each HRTEM image). The FT patterns of nanoparticles show Debye-Scherrer rings belonging to the orthorhombic InOOH (green) and rh-In₂O₃ (blue) phases. Some diffraction rings, which can be attributed to both, the InOOH and rh-In₂O₃ phases, are drawn in rose. We note that the starting particles are massive spheres with a (pure) orthorhombic InOOH structure. The nanoparticle ensemble still contains particles with InOOH and rh-In₂O₃ structure after 2 min illumination with an electron dose of $8.5 \cdot 10^7 \text{ e} \cdot \text{nm}^{-2}$ indicating that the phase transition is not finished. This is in contrast to the single

InOOH particle in Figure 5 (main text), where the InOOH-to-In₂O₃ phase transition is completed after 2 min illumination with an electron dose of 1.5·10⁸ e·nm⁻². Further electron illumination leads to the complete phase transition of the nanoparticle ensemble after 4 min illumination (electron dose of 1.7·10⁸ e·nm⁻²). Extended illumination (10 min) will result only in an improvement of the sphere-to-hollow sphere morphology without further phase transformation.

References

1. L. Schlicker, M. F. Bekheet and A. Gurlo, *Z Krist-Cryst Mater*, 2017, **232**, 129-140.
2. A. Doran, L. Schlicker, C. M. Beavers, S. Bhat, M. F. Bekheet and A. Gurlo, *Rev Sci Instrum*, 2017, **88**.
3. A. P. Hammersley, *ESRF Internal Report, ESRF97HA02T*, 1997.
4. A. P. Hammersley, S. O. Svensson, M. Hanfland, A. N. Fitch and D. Hausermann, *High Pressure Res*, 1996, **14**, 235-248.
5. J. I. Langford, D. Louer and P. Scardi, *J Appl Crystallogr*, 2000, **33**, 964-974.
6. N. C. Popa and D. Balzar, *J Appl Crystallogr*, 2002, **35**, 338-346.
7. R. F. Egerton, P. Li and M. Malac, *Micron*, 2004, **35**, 399-409.
8. V. I. Brinzari, A. I. Cocemasov, D. L. Nika and G. S. Korotcenkov, *Applied Physics Letters*, 2017, **110**.
9. T. Malis, S. C. Cheng and R. F. Egerton, *J Electron Microsc Tech*, 1988, **8**, 193-200.
10. L. Reimer and H. Kohl, in *Transmission Electron Microscopy*, Springer, 5-th edn., 2008, p. 462.
11. F. Seitz and J. S. Koehler, *Solid State Phys*, 1956, **2**, 305-448.
12. B. Darwent de B., Bond dissociation energies in simple molecules, <https://nvlpubs.nist.gov/nistpubs/Legacy/NSRDS/nbsnsrds31.pdf>, (accessed May 6, 2019).